RESEARCH ARTICLE SUMMARY

MARINE LIPIDS

Microbial dietary preference and interactions affect the export of lipids to the deep ocean

Lars Behrendt*†, Uria Alcolombri†, Jonathan E. Hunter†, Steven Smriga, Tracy Mincer, Daniel P. Lowenstein, Yutaka Yawata, François J. Peaudecerf, Vicente I. Fernandez, Helen F. Fredricks, Henrik Almblad, Joe J. Harrison, Roman Stocker*, Benjamin A. S. Van Mooy*

INTRODUCTION: Phytoplankton, through photosynthesis, convert carbon dioxide into particulate biomass. The subsequent sinking of phytoplankton-derived particles is a major biogeochemical pathway for the export of carbon from the atmosphere to the deep sea. Bacteria degrade particles during their descent, which fundamentally regulates the magnitude of this pathway. A substantial portion of phytoplankton biomass is composed of lipid molecules, which are vital for plankton energy storage and cellular functions. However, the mechanisms by which bacterial communities degrade these lipids during particle descent and how their degradation is influenced by microbial ecological factors remain largely unknown. This study addresses this limitation by employing a novel approach that combines nanoscale lipidomics and microscopy-based imaging to investigate the degradation of molecularly diverse phytoplankton-derived lipid droplets by bacteria isolated from sinking particles.

RATIONALE: Current understanding of lipid degradation in sinking particles focuses mostly on changes in lipid content with depth. However, the specific microscopic mechanisms by which distinct bacterial populations target and degrade different lipid molecular classes are not well characterized. This study sheds light on these dynamics by investigating bacterial dietary preferences for different lipid molecules, linking preferences to genes, examining community interaction effects using laboratory-based growth experiments, and finally developing a mathematical model that incorporates these findings to predict how bacterial communities affect lipid export to the deep sea.

RESULTS: By isolating bacteria from sinking particles and exposing them to phytoplankton-derived lipid droplets, the study revealed distinct dietary preferences among these bacterial populations. Some bacteria were highly selective and targeted specific lipid classes whereas others were indiscriminate and degraded a wide range of lipids. These dietary preferences were not linked to the taxonomic origin of the bacteria but rather to the presence or absence of specific lipid degradation genes within their genomes. Lipid degradation rates and the delay in the onset of degradation generally varied according to dietary preference. The study revealed that interactions between different bacteria affected degradation rates and delays, highlighting the potential importance of microbial ecological factors affecting lipids. The results were incorporated into a mathematical model that demonstrated how the combination of dietary preferences and bacterial interactions might influence lipid degradation efficiency in the ocean and consequently the quantity of particulate carbon exported to the deep sea in lipid form.

CONCLUSION: This study provides insight into the intricate dynamics of bacterial lipid degradation in sinking particles in the ocean. By demonstrating the existence of distinct dietary preferences, linkages to degradation rates, and the impact of bacterial interactions, our research highlights the importance of considering microbial community structure when studying the fate of organic molecules in the ocean. Finally, the development of a model that incorporates these findings lays the groundwork for future investigation into how microbial communities influence the transfer efficiency of other organic matter to the deep sea, ultimately contributing to a better understanding of the oceanic carbon cycle. ∎
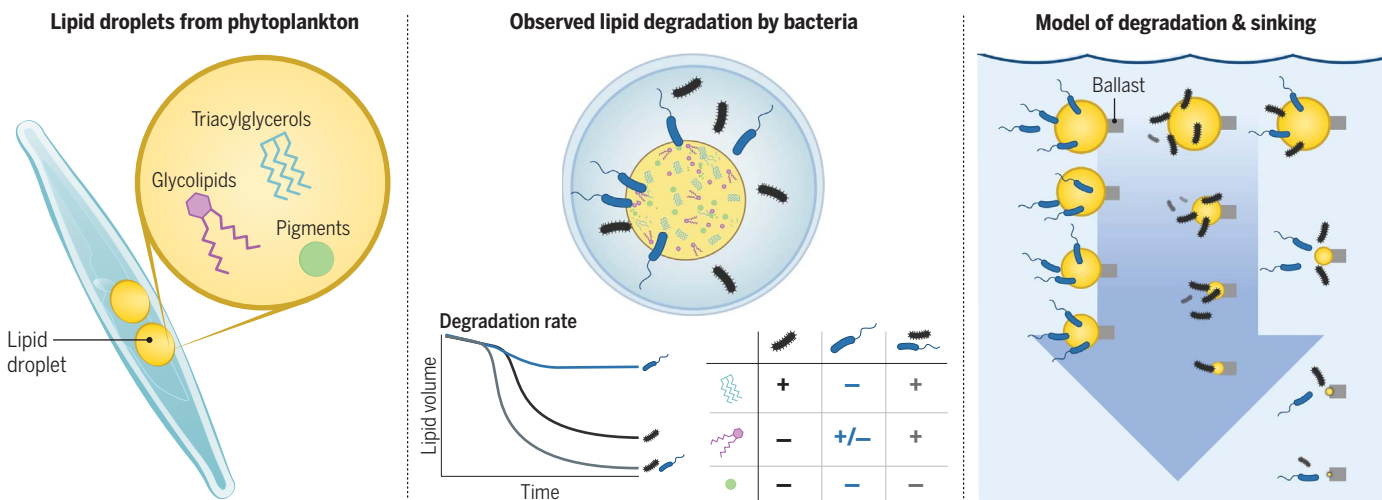
Bacterial degradation affects export of sinking lipids from phytoplankton. (Left) Lipid droplets containing diverse molecules were extracted from phytoplankton. (Middle) Droplets were exposed to bacteria that exhibited preferences for degrading lipid molecules at different rates, which changed when bacteria interacted. (Right) Modeled droplets (with ballast to cause sinking) showed how preferences and interactions might affect lipid export in the ocean.

MARINE LIPIDS

Microbial dietary preference and interactions affect the export of lipids to the deep ocean

Lars Behrendt[1]*†, Uria Alcolombri[2]†, Jonathan E. Hunter[3]†, Steven Smriga[4], Tracy Mincer[5], Daniel P. Lowenstein[3], Yutaka Yawata[6], François J. Peaudecerf[4,7], Vicente I. Fernandez[4], Helen F. Fredricks[3], Henrik Almblad[8], Joe J. Harrison[8], Roman Stocker[4]*, Benjamin A. S. Van Mooy[3]*

Lipids comprise a significant fraction of sinking organic matter in the ocean and play a crucial role in the carbon cycle. Despite this, our understanding of the processes that control lipid degradation is limited. We combined nanolipidomics and imaging to study the bacterial degradation of diverse algal lipid droplets and found that bacteria isolated from marine particles exhibited distinct dietary preferences, ranging from selective to promiscuous degraders. Dietary preference was associated with a distinct set of lipid degradation genes rather than with taxonomic origin. Using synthetic communities composed of isolates with distinct dietary preferences, we showed that lipid degradation is modulated by microbial interactions. A particle export model incorporating these dynamics indicates that metabolic specialization and community dynamics may influence lipid transport efficiency in the ocean's mesopelagic zone.

arbon export in the ocean is mediated primarily by the sinking of particles composed of biomolecules and biogenic minerals originating from plankton. As these particles sink, they transport particulate organic carbon (POC), originally assimilated in the euphotic zone by phytoplankton through photosynthesis, from the surface to the deep ocean, a process known as the biological pump. The microscale interactions of heterotrophic organisms such as bacteria and zooplankton with sinking particles are critical mechanisms constraining the magnitude of the biological pump (*1*), for example, by transforming POC into dissolved forms within the upper water layer and thereby reducing the flux of carbon into the deep ocean (*2*–*4*).

Approximately 5 to 30% of surface ocean POC is composed of lipids (*5*–*8*)—carbon-rich biomolecules used for energy storage, membrane structure, electron transport, and signaling (*9*). As POC sinks from the euphotic zone to the deep sea, it is degraded by diverse communities of resident microbes (*10*, *11*), making particles hotspots of cell abundance and activity of hydrolytic enzymes, including lipases involved in lipid degradation (*12*–*14*). The flux of lipids decreases by one order of magnitude as particles descend through the mesopelagic zone (*5*, *15*) contributing to the microbial release of CO_2 during remineralization. Thus, microbial lipid degradation on sinking particles exerts an important control on global CO_2 concentrations. Understanding the microscale processes that mediate microbial lipid remineralization in the ocean is therefore important for improving our ability to forecast global carbon fluxes in changing ocean regimes.

Aside from their contribution to POC, lipids are powerful markers for understanding sinking particles in the ocean. For decades, lipids were the primary biomarkers for assessing POC sources in the mesopelagic zone (*16*, *17*) and remain an important tool for understanding perturbations to the biological carbon pump (*18*). Many classes of lipids in plankton are highly labile and subject to molecular transformations that rapidly differentiate the lipid composition of sinking particles from that of living planktonic biomass (*19*–*21*). However, the mechanisms by which microbial communities degrade and ultimately remineralize lipids, and thereby attenuate the flux of this large component of POC through the mesopelagic zone, are poorly understood. Advanced marine lipidomics methods (*22*, *23*) have yet to be applied to this problem.

We combine nanoscale lipidomics with novel high-throughput fluorescence microscopy screening assays to show that bacteria isolated from natural sinking particles have distinct preferences for different classes of lipids. Using experiments with lipid droplets—models for lipid energy storage bodies in phytoplankton cells—we demonstrate that different bacteria degrade different lipids at considerably different rates. Furthermore, we also demonstrate that bacteria-bacteria interactions affect lipid remineralization rates. Using a mathematical model of sinking marine particles that incorporates bacterial degradation rates of lipid droplets, we show how microbial community structure could influence the transfer efficiencies of lipids from the euphotic zone to the deep sea.

Results and discussion

Lipid degradation dynamics are isolate specific

The lipid droplets were composed of lipids extracted from a 400-L culture of nitrogen-starved *Phaeodactylum tricornutum*, a marine diatom that forms conspicuous amounts of storage lipids upon nitrogen starvation (Fig. 1, A and B) (*24*). As marine plankton are typically under nitrogen limitation in the ocean (*25*), the composition of this lipid extract serves as a model for sinking aggregates formed by a declining diatom community. Using a recently developed, ultrasensitive lipidomic pipeline (*23*), we found that the diatom lipid extract was dominated by triacylglycerols (TAGs) and free fatty acids (FFAs), classes of lipid molecules that we found to also compose a large fraction of the lipids in sinking particles in the ocean (fig. S1) (*15*, *26*). The extract also contained smaller quantities of phospholipids (phosphatidylcholines), glycolipids [monogalactosyldiacylglycerols (MGDGs)], digalactosyldiacylglycerols, sulfoquinovosyldiacylglycerols, and chloropigments (chlorophyll *a* plus pheophytin *a*) (Fig. 1C).

We incubated individual droplets of diatom lipid extract (equivalent diameter 1.85 mm ± 0.21 mm, mean ± SD) with each of 24 isolates of bacteria: 21 isolates were grown from marine particles during a research cruise in Clayoquot sound (British Columbia) (*27*) and 3 are well-studied model isolates [*Ruegeria pomeroyi* DSS-3 (Rp3), *Marinobacter adhaerens* HP15 (Ma1), and *Alteromonas macleodii* ATCC 27126 (Am2); see table S1 for strain information]. Lipid content in droplets was measured after 11 days of incubation, revealing that bacteria do not degrade lipids indiscriminately, but rather that specific groups of bacteria selectively consume certain lipids (Fig. 2). Four "dietary" clusters emerged from this lipidomic analysis: Isolates in cluster I (*n* = 6) promiscuously degraded all lipids; isolates in cluster II (*n* = 4) degraded all lipids except TAGs; isolates in cluster III (*n* = 9) degraded only FFAs, TAGs, and MGDGs; and isolates in cluster IV (*n* = 5) degraded only FFAs. Membership of the different dietary clusters did not correlate

[1]Department of Organismal Biology, Science for Life Laboratory, Uppsala University, Uppsala, Sweden. [2]Department of Plant and Environmental Sciences, Institute of Life Sciences, The Hebrew University of Jerusalem, Jerusalem, Israel. [3]Department of Marine Chemistry and Geochemistry, Woods Hole Oceanographic Institution, Woods Hole, MA, USA. [4]Institute of Environmental Engineering, Department of Civil, Environmental and Geomatic Engineering, Eidgenössische Technische Hochschule Zürich (ETHZ), Zürich, Switzerland. [5]Florida Atlantic University, Wilkes Honors College, Jupiter, FL, USA. [6]Faculty of Life and Environmental Sciences, University of Tsukuba, Tsukuba, Japan. [7]University of Rennes, CNRS, Institut de Physique de Rennes, Rennes, France. [8]Department of Biological Sciences, University of Calgary, 2500 University Drive NW, Calgary, Alberta, Canada.
*Corresponding author. Email: lars.behrendt@scilifelab.uu.se (L.B.); romanstocker@ethz.ch (R.S.); bvanmooy@whoi.edu (B.A.S.V.M.)
†These authors contributed equally to this work.
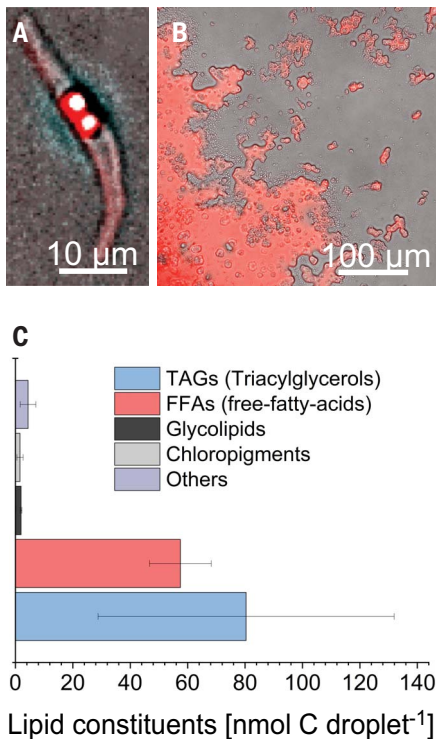
Fig. 1. The lipid content of nitrogen-starved diatoms is dominated by triacylglycerols and free fatty acids. (**A**) A single cell of the marine diatom *Phaeodactylum tricornutum* stained with the lipid-specific stain Nile red. (**B**) Lipid extracts from N-starved *P. tricornutum* cells adhere as droplets to a glass slide. Red fluorescence is due to the coextraction of autofluorescent chloropigments. (**C**) The major lipid constituents of the extract from N-starved *P. tricornutum* cells; "others" represents the sum of phospholipids, quinones, and other minor lipids detected by our analytical method (*23*). This lipid extract was used in all experiments unless indicated otherwise. Shown are the means (± SD) from five technical replicates.

with the taxonomic origin of the isolates (fig. S2). Instead, comparative genomics among four selected isolates from each dietary cluster [Am2 from cluster I, Rp3 from cluster II, *Pseudomonas zhaodongensis* (Pz15) from cluster III, and *Pseudoalteromonas shioyasakiensis* (Psh20) from cluster IV] revealed a distinct repertoire of putative TAG and fatty acid degradation (*fad*) genes (fig. S3). In particular, the copy numbers of *fad* gene paralogs, predicted to encode enzymes that catalyze the β-oxidation of prominent fatty acids (including FFAs; fig. S3), varied greatly among the genomes of the sequenced isolates from the four dietary clusters. Together, these data indicate that marine bacteria have distinct dietary preferences for specific fractions of diatom lipids and that similar degrader phenotypes emerge from different genomic backgrounds rather than by taxonomic association.

We next sought to determine whether bacterial dietary preferences affect the degradation kinetics of lipid droplets. We combined fluorescence microscopy with time-resolved lipidomic analysis (movies S1 to S3) and focused on the degradation behavior of two bacterial isolates distinguished by their divergent ability to degrade TAGs, the dominant lipid class in the extract from *P. tricornutum*. The two isolates were Rp3, an isolate from cluster II which cannot degrade TAGs, and Pz15, an isolate from cluster III which degrades TAGs (Fig. 2, both isolates indicated by black arrows). Time-lapse microscopy imaging of lipid droplets incubated with Pz15 (Fig. 3A) revealed that the autofluorescence of chloropigments (chlorophyll plus pheophytin) in lipid droplets decreased by an average of $19 \pm 5.3\%$ ($n = 5$) within 15 hours and remained low for the rest of the experiment. In comparison, in lipid droplets incubated with Rp3 the autofluorescence decreased by only $4.4 \pm 2.0\%$ after 42 hours ($n = 6$), similar to the no-bacteria control ($4.4 \pm 1.0\%$, $n = 3$, Fig. 3B).

Notably, despite the observed decrease in autofluorescence, the nanolipidomics analysis revealed that chloropigments were not degraded by either isolate. We ascribe the loss of autofluorescence during the course of degradation to the well-documented concentration-dependent self-quenching of chlorophyll molecules in highly concentrated solutions (*28*, *29*), (fig. S4 and movie S4). Essentially, the relative concentration of chloropigments in the droplet increased as TAGs, FFAs, and other lipids were degraded, resulting in self-quenching of chloropigment autofluorescence that is correlated with the loss of lipids. Parallel analysis of lipid droplets using nanolipidomics revealed that Pz15 degraded the total diatom-derived lipid pool almost completely within 48 hours, from an initial 158 ± 42 nmol C droplet^{-1} (mean ± SD, $n = 3$ per time point) to 24 ± 16 nmol C droplet^{-1}, corresponding to an 84% reduction (Fig. 3A). By contrast, Rp3 only degraded the total lipid pool from an initial 110 ± 22 to 72 ± 18 nmol C droplet^{-1}, corresponding to a 34% reduction (Fig. 3B). This difference in total lipid degradation between both isolates was also reflected in different amounts of phospholipids produced by the growing bacteria in their cell membranes; phospholipids were the dominant lipids in both isolates and generally distinct from phospholipids in the droplets (see supplementary materials and fig. S5). For Pz15, phospholipids increased from an initial 0.3 ± 0.1 nmol C droplet^{-1} to 5.4 ± 4.1 nmol C droplet^{-1} during 48 hours, reflecting a 1490% increase (Fig. 3C); for Rp3, by contrast, phospholipids increased from an initial 0.24 ± 0.1 nmol C droplet^{-1} to 0.7 ± 0.0 nmol C droplet^{-1} over 48 hours, corresponding to a 220% increase (Fig. 3D). We note that Rp3 also produces ornithine lipids, which were

not rigorously quantified as part of this study. Combined chloropigment autofluorescence and lipidomic measurements (Fig. 3, A and B) revealed that quenching of chloropigment autofluorescence is a good proxy for lipid degradation and that the total content of lipids in a droplet decreased linearly with decreasing fluorescence intensity (figs. S6 and S7). Together, these data on both isolates demonstrate that differences in their dietary preferences for lipids have a major impact on rates of lipid droplet degradation and consequentially on isolate growth rates.

In parallel with time-resolved fluorescence microscopy, our nano-lipidomic analysis enabled us to track the sequence of TAG and FFA degradation by Rp3 and Pz15 within single droplets of lipid extract (Fig. 3, C and D). Here, Pz15 degraded TAGs from an initial 80 ± 25 nmol C droplet^{-1} to 0.8 ± 0.7 nmol C droplet^{-1} during the first 16 hours (a 99% reduction) while concurrently also degrading FFAs (initial 67 ± 12 nmol C droplet^{-1} to 3.4 ± 0.6 nmol C droplet^{-1}, a 94% reduction; Fig. 3C). By contrast, during the first 16 hours, Rp3 did not degrade TAGs (49 ± 14 nmol C droplet^{-1} to 48 ± 18 nmol C droplet^{-1}), but degraded FFAs (initial 52 ± 10 nmol C droplet^{-1} to 12 ± 4 nmol C droplet^{-1}, a 77% reduction; Fig. 3D). These results recapitulate the findings from our initial screening of isolates (Fig. 2), and additionally show that Pz15 expresses its specific lipid degradation enzymes even at the initial stages of degradation. Thus, the dietary preference for different classes of lipids appears to be dictated by the inherent metabolic capabilities of each isolate and, at least in this study, not by the changing composition of the lipid droplet upon degradation. To better understand the origin of the dietary preference for these two isolates, we constructed and compared lipid degradation pathways in silico from the genomes of Pz15 and Rp3 (fig. S3). We found that the two isolates had distinct sets of lipid degradation enzymes, including a different set of acyl-CoA dehydrogenases. In addition, Pz15 possesses a triacylglycerol lipase, which is necessary for TAG degradation, whereas Rp3 lacks this enzyme. By contrast, both Pz15 and Rp3 genomes possess multiple paralogs for genes encoding functions that are predicted to drive FFA degradation. This suggests that the differences in lipid degradation are primarily associated with differences in the genetic repertoire of isolates (fig. S3), which might be the result of selective forces leading to diversification in lipid degradation strategies within bacteria inhabiting the mesopelagic.

The onset of rapid lipid degradation by Pz15 often occurred after a time delay, typically 7 to 12 hours (Fig. 3A). To understand the origin of this delay, we engineered Pz15 to constitutively express green fluorescent protein (GFP) from a plasmid and used fluorescence microscopy

Fig. 2. Marine bacteria exhibit distinct dietary preferences for different groups of phytoplankton lipids. Heatmap showing the degradation of different lipid fractions after incubation with bacterial monocultures (*n* = 24; species names and abbreviations are indicated at the bottom). Shown are fold changes in lipid content after 11 days of incubation. The different lipid constituents and their classification within major lipid groups are indicated by colored stars on the right of the heatmap. A nearest-neighbor clustering of the degradation profiles (i.e., the change in lipid content across the different lipid groups) revealed four clusters (I to IV), each characterized by different lipid fractions that were degraded to varying degrees by incubation with bacterial monocultures. Black arrows denote Rp3 and Pz15, two isolates selected for further biochemical and behavioral characterization (Figs. 3 and 4). Green arrows indicate additional isolates chosen as archetypical cluster representatives in experiments to quantify pairwise interactions when in co-culture with either Rp3 or Pz15 (Fig. 5).
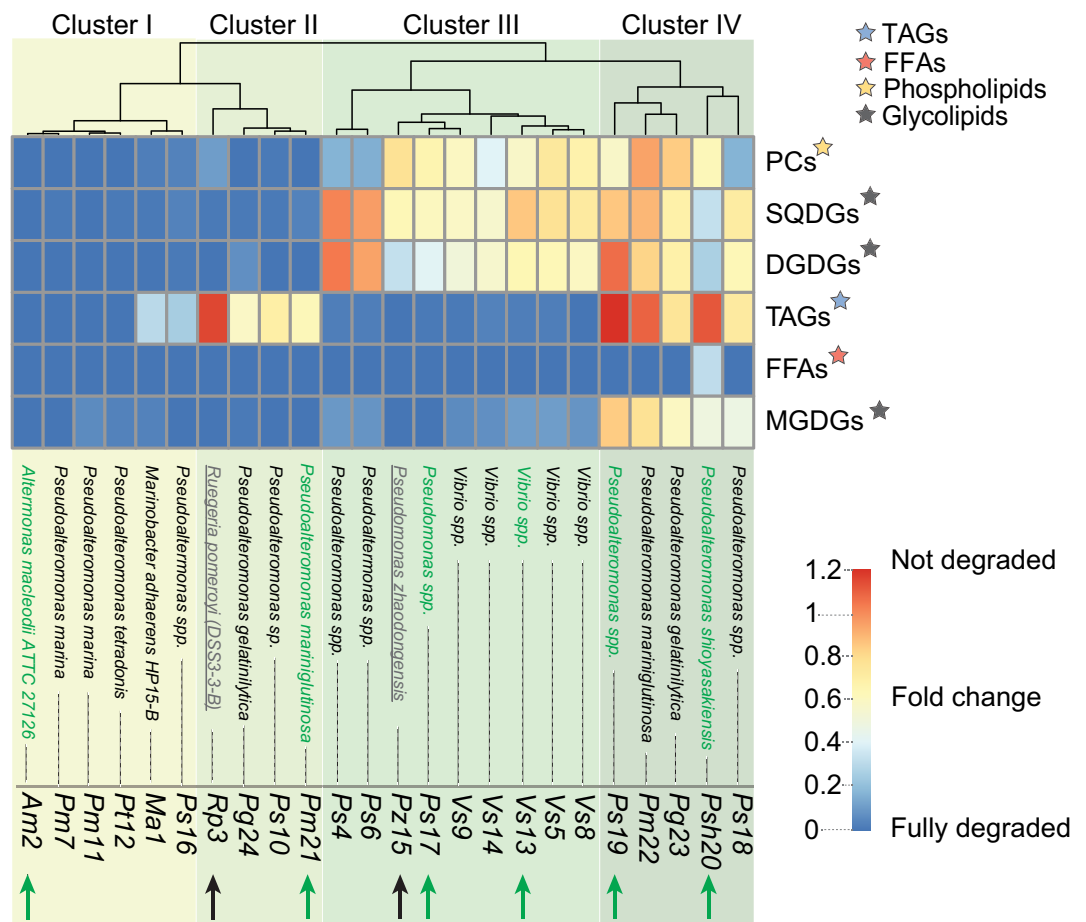
to investigate the microscale dynamics of lipid droplet degradation. This investigation revealed that only a small number of Pz15 cells immediately attached to the droplet upon inoculation whereas most of the colonization was delayed (movie S5). When GFP-labeled Pz15 cells were provided with a droplet composed of a synthetic TAG mixture (tripalmitoleic acid, three 16:1 fatty acids), motility and chemotaxis became prominent after a 10-hour delay and motile bacteria formed high concentrations of bacterial clusters on the droplet (movie S6). We attribute this behavior to the degradation-induced release of the glycerol moiety from TAGs to which *P. zhaodongensis* is chemoattracted (fig. S8) and which is likely released during the cleavage of TAGs. This result highlights that early bacterial colonizers are important for lipid degradation not only because of direct degradation but also because they can attract further degraders through the release of degradation products or metabolites that can act as chemoattractants (*30*).

Microbial interactions modulate the rate of lipid remineralization

We next set out to examine whether the correlation between dietary preference and deg-

radation rate in Pz15 and Rp3 extended to other bacteria isolated from particles. To do so, we chose six additional isolates as representatives of the different dietary clusters (Fig. 2, green arrows) and measured their degradation dynamics in shorter-term experiments (48 hours). The relationship between chloropigment autofluorescence and total lipids allowed us to use fluorescence as a time-resolved readout of lipid degradation in a high-throughput fluorescence plate-reader assay (figs. S6 and S7). From the resulting fluorescence curves we could estimate the delay before the onset of degradation and the maximum degradation rate (fig. S9). By plotting the maximum degradation rate against the delay in the onset of degradation (Fig. 4), we found that the selected isolates largely clustered according to their dietary preference previously determined in lipidomic experiments (Fig. 2). The fastest degradation rate [7.0 ± 0.9 nmol C (droplet h)$^{-1}$, *n* = 10] was exhibited by Am2 (Fig. 4), belonging to dietary cluster I (i.e., degrading all lipid constituents; Fig. 2). Slower degradation rates in the range of 2.3 to 5.3 nmol C (droplet h)$^{-1}$ [mean 3.8 ± 0.9 nmol C (droplet h)$^{-1}$, *n* = 26] were exhibited by Pz15, *Vibrio spp.* (Vs13) and *Pseudomonas spp.* (Ps17) (Fig. 4), belonging to dietary cluster

III (i.e., degrading three of the six detectable lipid classes: FFAs, TAGs and MGDGs; Fig. 2). These three isolates showed delay times in the range of 7.8 to 17.3 hours (13.0 ± 2.6 hours, *n* = 26). The longest delay (>48 hours) was exhibited by two *Pseudoalteromonas* isolates (Ps19, Psh20), belonging to dietary cluster IV (i.e., only degrading FFAs; Fig. 2). We note that this fluorescence plate-reader assay could not resolve the short-term lipid degradation kinetics of the most fastidious isolates. Specifically, we observed lipid degradation by *R. pomeroyi* in only 3 of 18 replicates (Fig. 4), whereas no measurable degradation occurred for *P. mariniglutinosa* (Pm21) over the 48-hour experiment. This suggests that Rp3 and Pm21 require longer timescales to degrade lipids fully and are not as capable of degrading lipids over shorter timescales, a result that, for Rp3, is consistent with our earlier experimental evidence (Fig. 3, B and D). Overall, the recapitulation of the dietary clusters in bacterial degradation kinetics suggests that lipid degradation by single isolates in the marine environment is fundamentally linked to their dietary preference.

To understand how dietary preference also affects degradation rates by multispecies

Fig. 3. Marine bacteria have widely different lipid degradation kinetics. (**A**) and (**B**) The degradation of *P. tricornutum* lipid extracts over 48 hours when incubated with Pz15 (left) or Rp3 (right). Microscopy images show representative lipid droplets at the beginning of the time course (0 hours) and near the end (42.5 hours). Scale bar is 100 μm. For each time point, the total lipid content (left axis) and chloropigment autofluorescence (right axis) of individual lipid droplets was quantified using automated lipidomics and fluorescence microscopy, respectively. Average normalized fluorescence for bacterial treatments (pink solid line) and for background controls (black dashed line) are shown ($n = 3$, SD not displayed due to large variance). Total lipid content per droplet is shown as mean ± SD ($n = 3$) for Pz15 [black triangles in (A)], Rp3 [black circles in (B)] and a no-bacteria control [gray squares in (B)]. Lipid contents after microscopy image correction (caused by sample handling, see fig. S7) are shown as smoothed dotted lines for Pz15 [black dotted line in (A)], Rp3 [black dotted line in (B)] and a no-bacteria control [gray dotted line in (B)].

(**C**) and (**D**) The lipidomic composition of lipid droplets in (A) and (B) upon incubation with Pz15 (left) and Rp3 (right). Shown are the fractions of TAGs (blue), FFAs (red), glycolipids (black), chloropigments (gray), and phospholipids (yellow) in percent of total lipids. Note that trace (<1%) amounts of lipids in other categories (e.g., betaine lipids, ornithine lipids, quinones, etc.) are not displayed. Shown in all figures are the means (± SD) from three replicates.
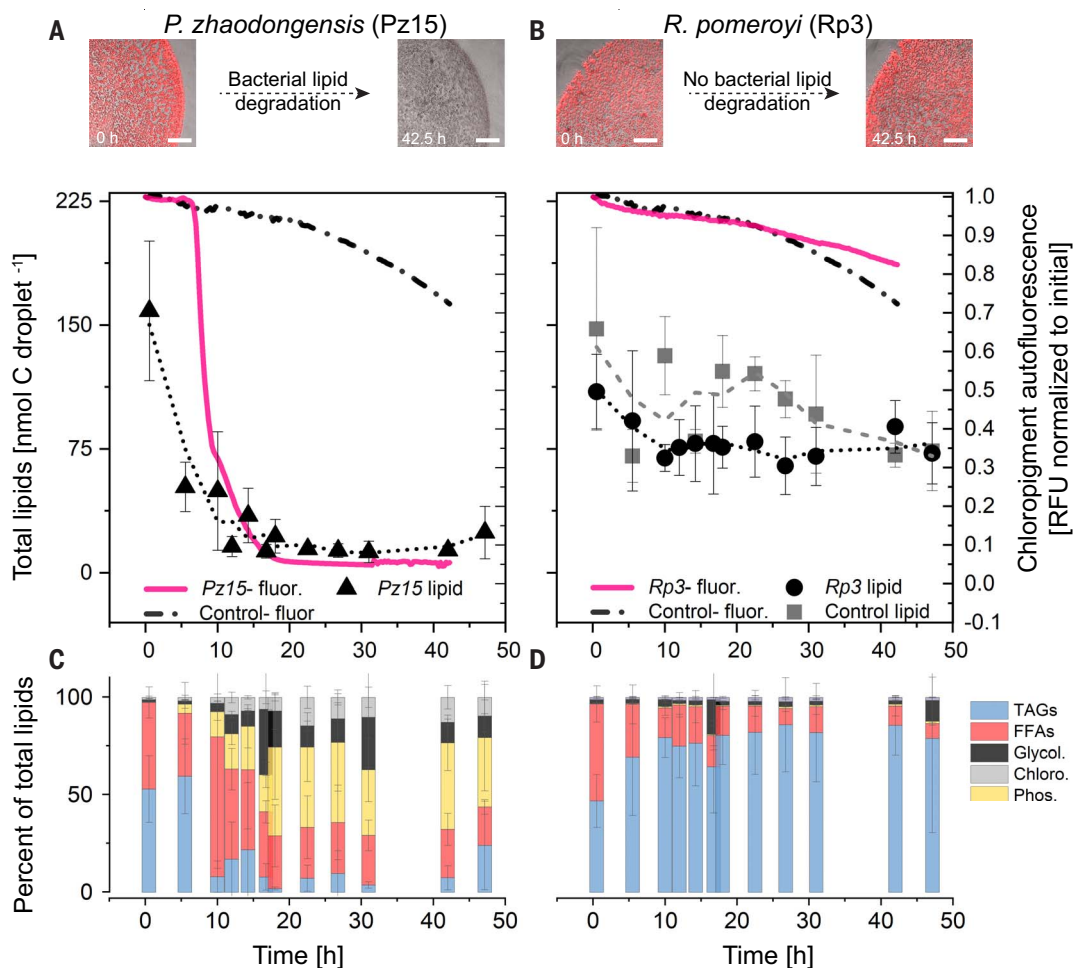
communities of bacteria, which are ecologically more relevant than species in isolation, we investigated the effect of pairwise interactions on lipid droplet degradation through the plate-reader assay. In experiments in which either the fast-degrader isolate Pz15 or slow-degrader Rp3 were inoculated together with single representative isolates chosen from the four dietary clusters (Fig. 2, green arrows), we found that simple synthetic co-cultures exhibited different degradation rates and delay times when compared to monocultures at the same cell density. Synergistically faster lipid degradation rates (two-sample *t*-test, $P < 0.05$) were observed when Pz15 was combined with Am2, Vs13, or Ps17 (Fig. 5A, $n = 6$ to 7 per combination), resulting in a 16 to 57% higher maximal degradation rate when compared to normalized monoculture rates. By contrast, no significant changes in maximum degradation rates were observed in pairwise interactions that included Rp3 (Fig. 5B, $n = 9$ to 10 per combination). The time delay was also

affected by pairwise interactions. We found significantly shorter delays when the isolates were co-cultured with Pz15 when compared to their respective monocultures (Fig. 5C, $n = 6$ to 7 per combination). By contrast, Rp3 co-cultures showed consistently longer delay times (Fig. 5D, $n = 9$ to 10 per combination).

The results from these experiments indicate that specific members of simple communities can accelerate or delay the overall lipid degradation compared to single isolates. To gain further insight into the nature of these interactions, we used fluorescence microscopy to investigate lipid degradation by GFP-labeled Pz15 co-cultured with Am2, a combination that yielded the shortest delay time and highest maximum degradation rate among all combinations of isolates tested (Fig. 5). For this simple consortium, we observed a well-mixed distribution of both isolates on the droplet (movie S7), potentially indicating syntrophy and the sharing of public goods (*31*) rather than, for example, the formation of segregated

patches. *Pseudomonas* relatives are known to be nutritionally versatile and to metabolize many carbon-rich compounds, including crude oil, oil derivatives (*32*), and aliphatic compounds (*33*), which suggests that simultaneous exploitation of similar lipid constituents—rather than a sequential consumption of each constituent by itself—could have caused faster degradation rates and shorter delay times in communities that include Pz15. Pairwise interactions with Rp3 (Fig. 5D) led to extensive delays in degradation. These delays are similar to those observed in interactions between secondary and primary degraders of simple synthetic polysaccharide particles (*34*) and may be due to the physical blockage of the lipid surface or, alternatively, to the production of secondary metabolites—a common phenomenon in *Rhodobacter* species (*35*, *36*). Our results, based on complex mixtures of compounds from plankton-derived lipid extracts, demonstrate that dietary preferences and microbial interactions at the scale of individual

Fig. 4. The lipid degradation kinetics of single bacterial isolates recapitulate their long-term degradation behavior. The kinetics of lipid droplet degradation derived from fluorescence time series for eight bacterial isolates (Pz15, Rp3, Vs13, Ps17, Am2, Ps19, Psh20, and Pm21) in monocultures, taken to be representative of the different dietary clusters (see Fig. 2, green arrows). Cluster affiliation is indicated following the descriptor of the bacterial isolate [e.g., "Pz15 (III)", indicates the placement of *P. zhaodongensis* in cluster III]. Maximum degradation rates and delay times were measured in two independent experiments (n = 4 to 10 for each isolate, designated by individual dots). Interrupted circles in boxed legend (cluster IV, bottom right) denote isolates with delay times >48 hours. Ellipsoids indicate the members of the dietary clusters from Fig. 2 and are labeled according to their cluster affiliation. Ellipses demark one standard deviation from a two-dimensional Gaussian fit to each isolate specific data.
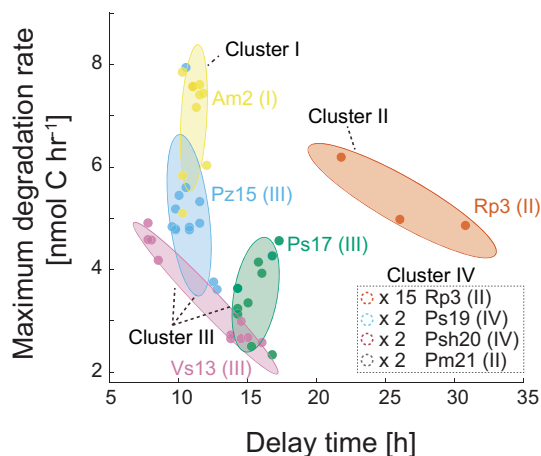
particles together control the rate of lipid remineralization by marine bacteria.

Potential implications of microbial interactions on oceanic lipid transport

Using our experimentally measured lipid droplet degradation dynamics, we developed a mathematical model to assess the potential effect of microbial interactions on vertical lipid transport in the ocean (supplementary model, fig. S10). The model tracks the sinking of individual particles from a size distribution that reflects the marine environment. Each particle contains a fixed proportion of lipid droplet and mineral ballast (37) and sinks at a speed that depends on its size and density as it descends from the base of the euphotic zone. Our model differs from recent single-particle approaches (3, 38) in that it considers two distinct phases within a particle: a lipid droplet phase (density = 8.8×10^5 g m^{-3}) that can be degraded by bacteria and a ballast phase (density = 2.35×10^6 g m^{-3}) that cannot. As lipid (but not ballast) is consumed, degradation leads to an increase in the particle density and thus sinking speed. As lipids are immiscible with water, likely limiting bacterial growth and degradation to the lipid–water interface (39–41), we assume a pseudo–first-order rate law, in which the absolute rate of lipid degradation is dependent on the surface area of the lipid droplet phase exposed to colonization. To calculate a range of possible values for the lipid degradation rate per unit of exposed lipid droplet surface (k_A; mol C m^{-2} s^{-1}), we combined the observed total degradation rates from our experiments with multiple isolates (Fig. 4; expressed as mol s^{-1} and dependent on the size of the observed droplet) together with our data of lipid droplet surface area (m^2) from the same experiments. Since these two

datasets are not paired, i.e., degradation rate and surface area were not measured on the same droplet, we used a Monte-Carlo approach to sample both datasets to obtain a representative distribution of degradation rates per unit area k_A (fig. S10A). We run the model using a range of bacterial degradation rate constants (k_A = 2×10^{-6} to 1×10^{-4} g m^{-2} s^{-1}) and a range of degradation delay times (t_{delay} = 0, 6, 12, 24 hours), spanning the ranges observed in our experiments for these parameters. By simultaneously tracking the degradation of the lipid phase in each particle and the depth of the particle (as determined by its sinking speed), the model computes the particle concentration and the lipid content per particle at any given depth. From this, we quantify the transfer efficiency of the vertical lipid flux, defined as the ratio of the lipid flux at depth z relative to the flux at the base of the euphotic zone z_0 (hereafter taken to be at z_0 = 100 m), for each particle size and over the entire particle population. The lower the transfer efficiency, the stronger is the attenuation of the lipid flux due to degradation by bacteria of the lipid phase.

The model predicts how microbial lipid degradation rates and delay times affect the lipid transfer efficiency of particles of different diameters containing lipid droplets. For smaller particles, the transfer efficiency is controlled almost exclusively by the degradation rate. Even when lipid degradation proceeds at the low end of the range of observed rates (k_A = 2×10^{-6} g m^{-2} s^{-1}), less than half of the lipid flux carried by particles <100 µm in diameter survive the descent to the bottom of the mesopelagic (1000 m depth). Furthermore, the delay in the onset of degradation has almost no effect on the transfer efficiency of small particles containing lipid, which can be inter-

preted as a direct consequence of their very slow sinking speed: For particles with 100-µm diameter, having an initial sinking speed of ~12 m day^{-1}, even the largest delay (24 hours) remains small compared to the time it takes for the particles to reach depths of hundreds of meters, and so the amount of degradation with and without delay is similar. By contrast, the delay has a much greater effect on larger, rapidly degrading particles which rapidly sink to depth. For example, if degradation is delayed by 24 hours, a particle with a diameter of 250 µm sinks almost unscathed through the top 100 m (as a result of its initial sinking speed of ~80 m day^{-1}), even when the highest degradation rate is considered. Conversely, without any delay 20% of the lipid in the particle will degrade over the same sinking distance of 100 m. Our model also provides estimates of total lipid transfer efficiencies (TEs) between an initial depth z_0 = 100 m and a final depth z = 1000 m (we call this TE$_{900}$) for the overall lipid flux, summed across an assumed initial size spectrum (42) of droplet sizes. We observed that TE$_{900}$ ranges from ~97% for the lowest degradation rate and longest delay to ~57% for the highest rate and no delay. Although the absolute values of the TE$_{900}$ are highly dependent on the initial size spectrum of sinking droplets in the model, and model calculation of TE$_{900}$ clearly illustrates the dependency of transfer efficiency on degradation rate and delay. This strong variation of transfer efficiency (more than 10× more attenuation at the highest degradation rate than at the lowest) results from the wide range of degradation rates considered, stemming from varying synergistic or antagonistic impacts of the community's composition on degradation. While our model does not account for all factors involved in lipid flux attenuation (e.g., particle disaggregation) and is based on rates obtained in vitro rather than from the environment, it illustrates the importance of bacterial degradation in determining the fate of lipids within sinking particles. The model also provides mechanistic insight into which classes of particle size will be more sensitive to variations in degradation rates and the delay of degradation. For example, given that the observed transfer efficiency of both TAGs and free fatty acids through the mesopelagic is likely to be less than 10%, based on previously published field studies (5, 15) and our own data (fig. S1), our model evokes the hypotheses that synergistic bacterial degradation of lipids is common and that particles containing lipid droplets in the marine environment are more likely to be small and sink slowly.

By coupling the quantitative analysis of physical processes to the effects of bacterial community structure on chemical processes, on the scale of individual particles, our study provides new insights into the degradation

Fig. 5. Pairwise interactions among marine bacteria affect the maximum rate and delay time of lipid degradation. The kinetics of lipid droplet degradation for synthetic two-isolate communities containing Pz15 or Rp3 as focal isolates. (**A**) Two-isolate communities containing Pz15 demonstrate an increase in maximum degradation rates when compared to a monocultures of Pz15, Vs13, or Ps17. The maximum degradation rate is calculated as the slope of a linear regression line fitted between the onset of degradation and its completion (fig. S9). All rates are normalized to the maximum degradation rate in monoculture experiments and expressed as percent change. (**B**) Two-isolate communities containing Rp3 show no significant difference between maximum degradation rates when compared to the respective monocultures of Am2, Vs13, or Ps17. (**C**) Two-isolate communities containing Pz15 show a reduction in delay time when compared to a monoculture of Pz15, Vs13, or Ps17. The delay time was defined as the time from the start of the experiment to the onset of degradation (fig. S9). (**D**) Two-isolate communities containing Rp3 show an increase in delay time when compared to the respective monocultures of Am2, Pz15, Vs13, or Ps17. In all graphs, the white dots represent individual measurements (*n* = 6 to 10 per condition). An asterisk indicates statistically significant differences (two-sample *t*-test, *P* < 0.05, assuming equal but unknown variances) between treatments.
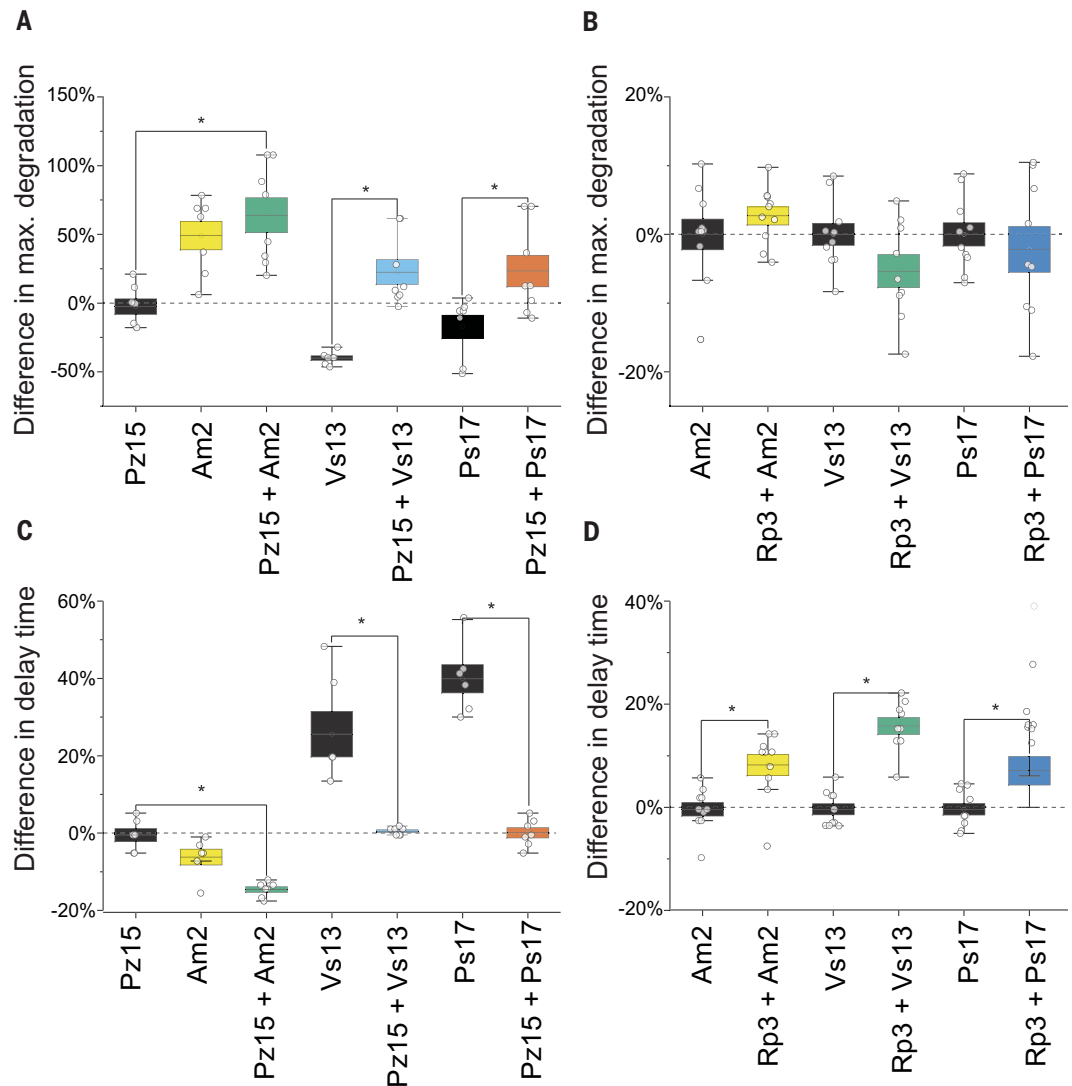
of sinking POC. POC degradation in the natural environment is much more complex than what is described in our study; to capture some of this complexity, we used a mixture of natural lipids from a phytoplankton culture rather than a single substrate, and studied the pairwise interactions of species rather than only species in isolation. It will ultimately be important to expand our findings to capture the full chemical complexity of natural POC in the ocean and the interactions among the often very rich community of microbial species residing on marine particles. Furthermore, the approach taken here—elucidating the connections between the molecular composition of POC, dietary preferences of bacteria for different molecules, and degradation kinetics—provides a blueprint for the study of the fate of phytodetritus, fecal pellets, and other organic carbon entities in the ocean. Results from such well-controlled, laboratory-based studies provide

the optimal ingredients to achieve a more mechanistic understanding of particle degradation and thus derive fundamental principles and laws that can inform large-scale models of the ocean carbon cycle.

Materials and methods
Phytoplankton growth

Cultures of *Phaeodactylum tricornutum* CCMP2561 were grown in a volume of 400 L of seawater based modified L1+Si medium in the facilities of the National Center for Marine Algae and Microbiota (NCMA, Bigelow, ME, USA). To generate N-starved cultures, L1 media was prepared as per standard recipe but NO_3 concentrations were adjusted to 1/16th of normal and Si concentrations to twofold normal. Small inoculum volumes were used to avoid media carryover which could potentially increase final NO_3 concentrations. Upon reaching mid-exponential growth, cells were harvested

by continuous centrifugation and the resulting pellet was frozen at −80°C, shipped on dry ice and used as input material in lipid extraction protocols (below).

Bacterial isolation, growth media, and physiological buffers

All marine bacterial isolates and strains are listed in table S1. Marine aggregates were collected in particle traps during a research cruise in Clayoquot sound (BC, Canada) (*27*). Collected aggregates were spread onto tryptone seawater agar plates (2% agar, 0.1% tryptone) and the resulting colonies were streaked to axenity. Individual clones were grown at 30°C in marine broth 2216 (Sigma Aldrich, 76448) augmented with sea salt to a salinity of 36 psu (Instant Ocean, Blacksburg, VA, USA) and agitated at 200 rpm before cryopreservation at −80°C with 10% DMSO. For experiments, cryopreserved bacteria were grown overnight

in marine broth 2216 at 30 °C and 200 rpm agitation. The resulting culture was centrifuged at 2350 g for 2 min and washed with sterile seawater-based f/2 medium (36 psu). This process was repeated 3 times and the washed culture was incubated at 30 °C for a minimum of 2 hours. After this starvation period, the optical density at 600 nm was measured on a spectrophotometer (BioTeK, Synergy HTX Multi-Mode Reader) and adjusted to 0.01 (corresponding to ~1 × 10^7 mL^{-1}). The final inoculation concentration of all bacterial cells in experimental setups was obtained by diluting the above washed culture into fresh f/2 medium. The concentrations of cells were either 2 × 10^6 cells mL^{-1} for the pairwise interaction experiments (see Pairwise interaction experiments) or 1 × 10^6 cells mL^{-1} for all other experiments. Where appropriate, bacteria were grown and propagated on lysogeny broth (LB, Thermofisher Scientific). Semi-solid agar media was prepared by adding 15 g L^{-1} bacto agar (Difco, Fisher Scientific) to LB or marine broth 2216. Alternatively, Zobell Marine Agar 2216 was purchased (Himedia, Mumbai, India) and prepared according to manufacturer's directions. Phosphate-buffered saline (PBS) was purchased as a 10× concentrated solution (Amresco, Solon, OH, USA) and diluted, as required, in sterile MilliQ-treated water.

Lipid extraction and droplet spotting

Bulk lipids were extracted from frozen, pelleted cells of *Phaeodactylum tricornutum* via a Bligh and Dyer extraction protocol (*43*). The resulting phytoplankton lipid extract was highly viscous, and lipid extracts were diluted in 99.5% Dichloromethane (Sigma Aldrich, D65100) at a w/v ratio of 1:100 to facilitate the dispensation of small volumes. Dispensation was done using a 100 μL glass Syringe (Hamilton 710N series, Hamilton Corp., Reno, NV, USA) connected to a 10 μL PCR glass micropipette (Drummond, Broomall, PY, USA) via Tygon (ND-100-80, Saint-Gobain Performance Plastics, Paris, France) tubing filled with deionized water. A PicoPlus syringe pump (Harvard apparatus, Holliston, MA, USA) was used to pre-load the glass micropipette with 10 μL of diluted lipid extracts and then used to spot lipid droplets by setting a 1 μL s^{-1} dispensation rate and a dispensation volume of 0.4 μL. Using this setup, lipid droplets were spotted by placing the tip of the glass micropipette in contact with the receiving glass surface and rapidly retracting the pipette. This resulted in lipid droplets with an equivalent diameter of 1.85 ± 0.21 mm (SD) and a height of ~ 10 μm as determined by confocal microscopy (Zeiss confocal, LSM 510 META). Lipid droplets were either spotted into the bottom of low-absorption LC-MS vials with a volume of 2 mL (Supelco, Bellefonte, PA, USA) or glass bottom 96-well plates (Cellvis, Mountain View, CA, USA),

depending on the experimental setup. Residual DCM was removed from the phytoplankton lipid by placing vials or plates under vacuum for >1 hours and lipid integrity was preserved by placing plates/vials with spots into −80 °C and using them within a day.

Lipid droplet visualization

Lipid droplets were found to strongly autofluoresce under an excitation/emission combination typically used for Cy5 imaging (Ex.: 628/40 nm HBW, Em.: 692/40 nm HBW). This autofluorescence is caused by co-extracted photopigments, i.e., chlorophyll *a* and *c* (*44*), and their chemical conversion to pheophytin. We exploited the natural lipid autofluorescence to estimate the degradation of lipids (see section on Lipid autofluorescence quenching as a proxy for lipid degradation) and to visualize the bacterial interactions occurring on lipid droplets. All lipid droplets were visualized on an automated fluorescence microscope (Nikon-Eclipse Ti, Nikon Corp., Tokyo, Japan) with excitation wavelengths provided by a Spectra X light engine (Lumencor, OR, USA). Temperature control was provided by an encasing incubator (Life Imaging Services, Basel Switzerland) and kept constant at 30°C for all experiments.

Initial screening of bacterial isolates for lipid degradation

In order to determine the ability of microbial isolates (*n* = 24) to degrade phytoplankton lipids, isolates were incubated in the presence of lipid droplets. For this, cells were dispensed into LC-MS vials (to a concentration of 1 × 10^6 mL^{-1}) containing lipid droplets and hereafter incubated at 30 °C. Immediately after dispensation, a first set of vials were sampled and frozen at −80 °C (= C_{-O} time point) and the remainder incubated for a total duration of 11 days before final endpoint sampling (= C_{-11} time point). All samples were kept at −80 °C after sampling and shipped in liquid N_2 filled dewars for chemical processing.

Combined microscopic imaging and lipidomic sampling

To combine physical observations with chemical sampling, LC-MS vials (2 mL) with lipid droplets and selected bacterial isolates were placed into a microscopy-compatible acrylic holder (Fig. S11). A volume of 50 μL bacteria was added to 450 μL f/2 media within LC-MS vials to achieve a final bacterial concentration of 1 × 10^6 mL^{-1} and a final volume of 500 μL. This allowed for the simultaneous microscopic imaging of dispensed lipid droplets and bacteria at the bottom of vials and facilitated their systematic sampling for fixation at specific time points after bacterial inoculation (see Fig. 3): 0.5, 5.5, 10, 12, 14.25, 16.75, 18, 22.5, 26.75, 31, 43, and 47.15 hours. At each of these time

points three replicate vials were removed and immediately placed into −80° C for subsequent lipidomic analysis. Due to space constraints on the microscopy stage, additional LC-MS vials were placed adjacent to the microscopy stage under identical conditions and collected for lipidomic analysis at identical times.

Lipids were extracted from LC-MS vials using a variation of the Bligh and Dyer (*43*) method described above. To the experiments containing 500 μL f/2 media with bacteria, 2 mL of methanol, 1 mL of dichloromethane, and 300 μL of phosphate-buffered saline were added. We then added dinitrophenyl phosphatidylethanolamine as an internal recovery standard, vigorously vortexed the vials, and sonicated them for 5 min. Next, 1 mL of dichloromethane and 1 mL of water were added. The resulting dichloromethane was transferred to another vial and butylated hydroxytoluene was added to prevent oxidation. Extracts were stored at −80 C prior to analysis.

Lipidomic analysis

All lipidomic analysis was done according to a previously described method (*45*). Nanoflow high-performance liquid-chromatography (nano-HPLC) was performed with a Thermo Scientific Easy nLC 1200 apparatus. Samples were injected in a direct mode onto a Thermo Scientific Acclaim PepMap 100 (75 μm × 2 cm; 3 μm; 100 Å), C18 guard column, and a Thermo Scientific Acclaim PepMap RSLC (75 μm × 15 cm; 2 μm; 100 Å) C18 analytical column, housed in a Phoenix S&T PST-BPH-20 butterfly column heater operated at 50°C. Prior to analysis, lipid extracts were blown down with N_2 to remove dichloromethane and then dissolved in 50% water and 50% isopropanol. Eluent A consisted of 75% water, 25% acetonitrile, 0.1% formic acid, and 0.04% ammonium hydroxide; Eluent B consisted of 75% isopropanol, 25% acetonitrile, 0.1% formic acid, and 0.04% ammonium hydroxide. The chromatographic gradient profile, at a constant flow rate of 300 nL min^{-1}, is defined in (*23*). Thermo Scientific Nanospray Flex source and stainless-steel emitter tip were used to couple the nano-HPLC system to a Q-Exactive orbitrap mass spectrometer. Data processing and annotation were performed using the LOBSTAHS (*45*). Lipids were quantified using external standard curves and internal recovery standards as described in detail before (*23*).

Lipid autofluorescence quenching as a proxy for lipid degradation

The quantification of lipid autofluorescence in parallel with nano-LC-MS lipidomic analysis revealed that the total amount of lipid present was approximately proportional to the magnitude of fluorescence (fig. S6). Lipid fluorescence quenching is mediated by the bacterial degradation of lipids and the concurrent accumulation

of co-extracted pheophytin, i.e. chlorophyll without Mg^{2+} ion. As some bacteria in our collection degraded lipids, but not pheophytin, the accumulation of pheophytin leads to a loss of autofluorescence by concentration dependent quenching mechanisms (*28*, *46*). These relationships (between measured fluorescence and chlorophyll concentration and between lipid content and chlorophyll concentration) were parameterized directly from experiments (fig. S6) and allowed us to relate both parameters and establish fluorescence as a non-invasive readout of lipid degradation.

To quantify lipid degradation, time series data was generated for Cy5 fluorescence data (Ex.: 628/40 nm HBW, Em.: 692/40 nm HBW) alongside abiotic droplet controls. Through comparison, the total bacterially degraded lipids were estimated (fig. S9). A smoothing spline with a five-hour window was then applied, identifying the time offset (delay) and magnitude of the highest degradation rate (fig. S9). This technique was applied to fluorescence dynamics for individual isolates, as well as for multispecies communities to enable a rapid screening assay.

Pairwise interaction experiments

In order to determine whether the interaction between bacterial isolates affects the degradation of phytoplankton lipid extracts, selected pairs of microbial isolates co-incubated in the presence of lipid droplets. For this, lipid droplets were spotted into glass-bottom 96-well plates and the isolates Pz15 or Rp3 were combined with selected bacterial isolates from the strain collection. Each isolate was added at a concentration of 1×10^6 mL^{-1}, always resulting in final concentrations of 2×10^6 mL^{-1} per reaction volume. For single-isolates in interaction experiments, the amount added was doubled to achieve a final concentration of 2×10^6 mL^{-1} per reaction volume. Using a fluorescence plate reader (BioTeK, Synergy HTX Multi-Mode Reader), the fluorescence decay of lipid droplets was observed using Cy5 specific excitation/emission (Ex.: 620/40 nm HBW, Em.: 680/30 nm HBW). Fluorescence was assessed at the bottom of each well every 15 minutes for a total duration of 48 h. Significance testing was conducted via two-sample *t*-tests assuming equal but unknown variances.

Mathematical model of vertical flux

We refer the reader to the SM for a description of the model.

REFERENCES AND NOTES

1. P. W. Boyd, H. Claustre, M. Levy, D. A. Siegel, T. Weber, Multi-faceted particle pumps drive carbon sequestration in the ocean. *Nature* **568**, 327–335 (2019). doi: 10.1038/s41586-019-1098-2; pmid: 30996317

2. T. T. H. Nguyen *et al.*, Microbes contribute to setting the ocean carbon flux by altering the fate of sinking particulates. *Nat. Commun.* **13**, 1657 (2022). doi: 10.1038/s41467-022-29297-2; pmid: 35351873

3. U. Alcolombri *et al.*, Sinking enhances the degradation of organic particles by marine bacteria. *Nat. Geosci.* **14**, 775–780 (2021). doi: 10.1038/s41561-021-00817-x

4. J. R. Collins *et al.*, The multiple fates of sinking particles in the North Atlantic Ocean. *Global Biogeochem. Cycles* **29**, 1471–1494 (2015). doi: 10.1002/2014GB005037

5. S. G. Wakeham, J. I. Hedges, C. Lee, M. L. Peterson, P. J. Hernes, Compositions and transport of lipid biomarkers through the water column and surficial sediments of the equatorial Pacific Ocean. *Deep Sea Res. Part II Top. Stud. Oceanogr.* **44**, 2131–2162 (1997). doi: 10.1016/S0967-0645(97)00035-0

6. J. I. Hedges *et al.*, Evidence for non-selective preservation of organic matter in sinking marine particles. *Nature* **409**, 801–804 (2001). doi: 10.1038/35057247; pmid: 11236989

7. R. Pedrosa-Pàmies, M. H. Conte, J. C. Weber, R. Johnson, Carbon cycling in the Sargasso Sea water column: Insights from lipid biomarkers in suspended particles. *Prog. Oceanogr.* **168**, 248–278 (2018). doi: 10.1016/j.pocean.2018.08.005

8. B. Gašparović *et al.*, Factors influencing particulate lipid production in the East Atlantic Ocean. *Deep Sea Res. Part I Oceanogr. Res. Pap.* **89**, 56–67 (2014). doi: 10.1016/j.dsr.2014.04.005

9. B. R. Edwards, Lipid Biogeochemistry and Modern Lipidomic Techniques. *Annu. Rev. Mar. Sci.* **15**, 485–508 (2023). doi: 10.1146/annurev-marine-040422-094104; pmid: 35878678

10. D. Boeuf *et al.*, Biological composition and microbial dynamics of sinking particulate organic matter at abyssal depths in the oligotrophic open ocean. *Proc. Natl. Acad. Sci. U.S.A.* **116**, 11824–11832 (2019). doi: 10.1073/pnas.1903080116; pmid: 31127042

11. B. Valencia *et al.*, Microbial communities associated with sinking particles across an environmental gradient from coastal upwelling to the oligotrophic ocean. *Deep Sea Res. Part I Oceanogr. Res. Pap.* **179**, 103668 (2022). doi: 10.1016/j.dsr.2021.103668

12. A. Krupke, L. R. Hmelo, J. E. Ossolinski, T. J. Mincer, B. A. S. Van Mooy, Quorum sensing plays a complex role in regulating the enzyme hydrolysis Activity of microbes associated with Sinking Particles in the ocean. *Front. Mar. Sci.* **3**, 1–9 (2016). doi: 10.3389/fmars.2016.00055

13. H.-G. Hoppe, H. Ducklow, B. Karrasch, Evidence for dependency of bacterial growth on enzymatic hydrolysis of particulate organic matter in the mesopelagic ocean. *Mar. Ecol. Prog. Ser.* **93**, 277–283 (1993). doi: 10.3354/meps093277

14. B. R. Edwards, K. D. Bidle, B. A. S. Van Mooy, Dose-dependent regulation of microbial activity on sinking particles by polyunsaturated aldehydes: Implications for the carbon cycle. *Proc. Natl. Acad. Sci. U.S.A.* **112**, 5909–5914 (2015). doi: 10.1073/pnas.1422664112; pmid: 25918397

15. S. G. Wakeham, E. A. Canuel, Organic geochemistry of particulate matter in the eastern tropical North Pacific Ocean: Implications for particle dynamics. *J. Mar. Res.* **46**, 183–213 (1988). doi: 10.1357/002224088785113748

16. S. G. Wakeham *et al.*, Organic matter fluxes from sediment traps in the equatorial Atlantic Ocean. *Nature* **286**, 798–800 (1980). doi: 10.1038/286798a0

17. J. J. Kharbush *et al.*, Particulate Organic Carbon Deconstructed: Molecular and chemical composition of particulate organic carbon in the ocean. *Front. Mar. Sci.* **7**, 518 (2020). doi: 10.3389/fmars.2020.00518

18. R. Pedrosa-Pàmies, M. H. Conte, J. C. Weber, R. Johnson, Hurricanes enhance labile carbon export to the deep ocean. *Geophys. Res. Lett.* **46**, 10484–10494 (2019). doi: 10.1029/2019GL083719

19. B. Gašparović, R. S. Lampitt, N. Sudasinghe, T. Schaub, Molecular-level evidence of early lipid transformations throughout oceanic depths. *Geochim. Cosmochim. Acta* **343**, 49–63 (2023). doi: 10.1016/j.gca.2022.12.021

20. J. M. Fulton, H. F. Fredricks, B. A. S. Van Mooy, Intact polar lipid export in the temperate western North Atlantic and Sargasso Sea. *Org. Geochem.* **114**, 45–56 (2017). doi: 10.1016/j.orggeochem.2017.09.005

21. J.-F. Rontani, S. T. Belt, Photo- and autoxidation of unsaturated algal lipids in the marine environment: An overview of processes, their potential tracers, and limitations. *Org. Geochem.* **139**, 103941 (2020). doi: 10.1016/j.orggeochem.2019.103941

22. H. C. Holm *et al.*, Global ocean lipidomes show a universal relationship between temperature and lipid unsaturation. *Science* **376**, 1487–1491 (2022). doi: 10.1126/science.abn7455; pmid: 35737766

23. J. E. Hunter *et al.*, Using high-sensitivity lipidomics to assess Microscale Heterogeneity in Oceanic Sinking Particles and Single Phytoplankton Cells. *Environ. Sci. Technol.* **55**, 15456–15465 (2021). doi: 10.1021/acs.est.1c02836; pmid: 34724376

24. J. Lupette *et al.*, The architecture of lipid droplets in the diatom *Phaeodactylum tricornutum*. *Algal Res.* **38**, 101415 (2019). doi: 10.1016/j.algal.2019.101415

25. C. M. Moore *et al.*, Processes and patterns of oceanic nutrient limitation. *Nat. Geosci.* **6**, 701–710 (2013). doi: 10.1038/ngeo1765

26. K. W. Becker *et al.*, Daily changes in phytoplankton lipidomes reveal mechanisms of energy storage in the open ocean. *Nat. Commun.* **9**, 5179 (2018). doi: 10.1038/s41467-018-07346-z; pmid: 30518752

27. L. R. Hmelo, T. J. Mincer, B. A. S. Van Mooy, Possible influence of bacterial quorum sensing on the hydrolysis of sinking particulate organic carbon in marine environments. *Environ. Microbiol. Rep.* **3**, 682–688 (2011). doi: 10.1111/j.1758-2229.2011.00281.x; pmid: 23761357

28. A. R. Kelly, L. K. Patterson, Model systems for photosynthesis. II. Concentration quenching of chlorophyll *b* fluorescence in solid solutions. *Proc. R. Soc. A Math. Phys. Eng. Sci.* **324**, 117–126 (1971).

29. J. Dalton, Concentration quenching in chlorophyll. *J. Chem. Soc. Chem. Commun.* **260**, 78 (1980). doi: 10.1039/c39800000078

30. R. Stocker, Marine microbes see a sea of gradients. *Science* **338**, 628–633 (2012). doi: 10.1126/science.1208929; pmid: 23118182

31. C. Ratzke, J. Gore, Self-organized patchiness facilitates survival in a cooperatively growing *Bacillus subtilis* population. *Nat. Microbiol.* **1**, 16022 (2016). doi: 10.1038/nmicrobiol.2016.22; pmid: 27572641

32. E. Kaczorek, T. Jesionowski, A. Giec, A. Olszanowski, Cell surface properties of *Pseudomonas stutzeri* in the process of diesel oil biodegradation. *Biotechnol. Lett.* **34**, 857–862 (2012). doi: 10.1007/s10529-011-0835-x; pmid: 22210557

33. J. Lalucat, A. Bennasar, R. Bosch, E. García-Valdés, N. J. Palleroni, Biology of *Pseudomonas stutzeri*. *Microbiol. Mol. Biol. Rev.* **70**, 510–547 (2006). doi: 10.1128/MMBR.00047-05; pmid: 16760312

34. T. N. Enke, G. E. Leventhal, M. Metzger, J. T. Saavedra, O. X. Cordero, Microscale ecology regulates particulate organic matter turnover in model marine microbial communities. *Nat. Commun.* **9**, 2743 (2018). doi: 10.1038/s41467-018-05159-8; pmid: 30013041

35. P. W. D'Alvise, J. Melchiorsen, C. H. Porsby, K. F. Nielsen, L. Gram, Inactivation of *Vibrio* anguillarum by attached and planktonic Roseobacter cells. *Appl. Environ. Microbiol.* **76**, 2366–2370 (2010). doi: 10.1128/AEM.02717-09; pmid: 20118354

36. L. L. Lindqvist *et al.*, Tropodithietic Acid, a Multifunctional Antimicrobial, Facilitates Adaption and Colonization of the Producer, *Phaeobacter piscinae*. *MSphere* **8**, e00517–e00522 (2023). doi: 10.1128/msphere.00517-22; pmid: 36622251

37. R. A. Armstrong, C. Lee, J. I. Hedges, S. Honjo, S. G. Wakeham, A new, mechanistic model for organic carbon fluxes in the ocean based on the quantitative association of POC with ballast minerals. *Deep Sea Res. Part II Top. Stud. Oceanogr.* **49**, 219–236 (2001). doi: 10.1016/S0967-0645(01)00101-1

38. M. M. Omand, R. Govindarajan, J. He, A. Mahadevan, Sinking flux of particulate organic matter in the oceans: Sensitivity to particle characteristics. *Sci. Rep.* **10**, 5582 (2020). doi: 10.1038/s41598-020-60424-5; pmid: 32221314

39. M. Zheng, W. Wang, K. Papadopoulos, Direct visualization of oil degradation and biofilm formation for the screening of crude oil-degrading bacteria. *Bioremediat. J.* **24**, 60–70 (2020). doi: 10.1080/10889868.2019.1671795

40. M. M. Yakimov, K. N. Timmis, P. N. Golyshin, Obligate oil-degrading marine bacteria. *Curr. Opin. Biotechnol.* **18**, 257–266 (2007). doi: 10.1016/j.copbio.2007.04.006; pmid: 17493798

41. J. Mounier *et al.*, The marine bacterium *Marinobacter hydrocarbonoclasticus* SP17 degrades a wide range of lipids and hydrocarbons through the formation of oleolytic biofilms with distinct gene expression profiles. *FEMS Microbiol. Ecol.* **90**, 816–831 (2014). doi: 10.1111/1574-6941.12439; pmid: 25318592

42. G. A. Jackson *et al.*, Particle size spectra between 1 μm and 1 cm at Monterey Bay determined using multiple instruments. *Deep Sea Res. Part I Oceanogr. Res. Pap.* **44**, 1739–1767 (1997). doi: 10.1016/S0967-0637(97)00029-0

43. E. G. Bligh, W. J. Dyer, A rapid method of total lipid extraction and purification. *Can. J. Biochem. Physiol.* **37**, 911–917 (1959). doi: 10.1139/y59-099; pmid: 13671378

44. J. E. Mann, J. Myers, On pigments, growth, and photosynthesis of *Phaeodactylum tricornutum*. *J. Phycol.* **4**, 349–355 (1968). doi: 10.1111/j.1529-8817.1968.tb04707.x; pmid: 27068211

45. J. R. Collins *et al.*, LOBSTAHS: An adduct-based lipidomics strategy for discovery and identification of oxidative stress biomarkers. *Anal. Chem.* **88**, 7154–7162 (2016). doi: 10.1021/acs.analchem.6b01260

46. G. S. Beddard, S. E. Carlin, G. Porter, Concentration quenching of chlorophyll fluorescence in bilayer lipid vesicles and liposomes. *Chem. Phys. Lett.* **43**, 27–32 (1976). doi: 10.1016/0009-2614(76)80749-X

47. L. Behrendt *et al.*, Microbial dietary preference and interactions affect the export of lipids to the deep ocean, Dryad (2024); https://doi.org/10.5061/dryad.xgxd254ps.

48. F. J. Peaudecerf, fpeaudecerf/pelagic_lipid_export: First release of pelagic lipid export code, Version v1.0.0, Zenodo (2024); https://zenodo.org/records/10809049.

ACKNOWLEDGMENTS

SUPPLEMENTARY MATERIALS